IEEE Access
Multidisciplinary | Rapid Review | Open Access Journal

Received February 3, 2019, accepted February 14, 2019, date of publication February 19, 2019, date of current version March 7, 2019.

Digital Object Identifier 10.1109/ACCESS.2019.2900256

Construction of Rate-Compatible Physical Layer Network Coding in Two-Way Relay Systems

YING YOU[1,2], ZHAOPENG XIE[2], PINGPING CHEN[2], (Member, IEEE), AND ZHIJIAN LIN[2]
[1]Department of Electronic and Information Engineering, Fuqing Branch of Fujian Normal University, Fujian 350300, China
[2]Department of Electronic Information, Fuzhou University, Fujian 350108, China

Corresponding author: Pingping Chen (ppchen.xm@gmail.com)

This work was supported in part by the NSF of Fujian under Grant 2017J01106, in part by the Education Scientific Research Project for Young Teachers of Fujian Province under Grant JAT170668 and Grant JT180053, in part by the University Key NSF Project of Fujian under Grant JZ160489, and in part by NSF of China under Grant 61871132.

ABSTRACT The existing physical-layer network coding (PNC) only considers channel codes of a constant coding rate. In this paper, we propose a rate-compatible (RC) channel coding scheme for PNC in two-way relay systems. Our contributions are as follows. First, we propose a two-edge-type-low-density-paritycheck-aided PNC (JTNC) scheme due to its simple implementation and excellent performance. Second, we design an RC scheme, i.e., choice of locations and symbols, for the proposed JTNC in the relay. The simulation results show that the proposed RC-JTNC has good error correction performance and achieves large gains over the existing puncturing algorithms aided PNC over a wide range of rates.

INDEX TERMS CLS, TET-LDPC codes, PNC, RC, JTNC, TWRS.

I. INTRODUCTION

Physical layer network coding (PNC) can improve the throughput significantly by exploiting the interference of user messages [1]–[3]. One basic application for PNC is wireless two-way relay systems (TWRS) [4]–[6]. Generally, PNC in TWRS consists of two phases: multiple access (MAC) and broadcast (BC). In the MAC phase, two users transmit their messages to a relay simultaneously. The relay helps two users to exchange messages and aims to decode the overlapped signals into network coded (NC) messages. The simplest form of NC messages is the XOR of two vectors which are encoded from two user's source messages [7]–[9].

Various channel codes have been applied in PNC to ensure communication reliability, such as repeat accumulate (RA) codes [9], irregular low-density-parity-check (LDPC) codes [10], [11] and Lattice codes [12]. Most of these channel-coded PNC systems assumed that the same linear channel code is used at two users. By doing so, the XOR of encoded vectors from two users, i.e., the XOR message is also a valid codeword of the channel code, which can be directly decoded from received signals by the sum product algorithm (SPA) [13], [14] or the log-likelihood-ratio (LLR) decoding algorithm [15].

The associate editor coordinating the review of this manuscript and approving it for publication was Rui Wang.

MET-LDPC codes, generalizations of the concept of regular and irregular LDPC codes, include various constructions and have excellent performance in threshold, adaptability and error floor [16]. As a kind of MET-LDPC codes, two-edge-type-low-density-parity-check (TET-LDPC) codes which have two edge types increase the stability of density evolution and facilitate simply encoding [17]. However, to the best of our knowledge, TET-LDPC codes have not been studied in PNC. Thus, this paper proposes a joint TET-LDPC aided PNC coding (JTNC) scheme and investigates the corresponding LLR decoding algorithm.

Rate compatible (RC) coding has been proposed as an effective capacity-enhancement method in wireless communication channels [18], [19]. RC can adjust the code rate and coding scheme according to different channel situations. In particular, RC codes can be realized from a mother code by puncturing and can be implemented by a single pair of encoder and decoder. RC codes have been integrated in many channel codes, such as convolutional codes [20], [21], irregular RA codes [22], LDPC codes [23], [24], quasi-cyclic LDPC codes [25], MET-LDPC codes [26].

In wireless communication systems, spectrum resources are scarce. To improve spectrum utilization and enhance the throughput, the coordination and optimization among physical layer, data link layer and network layer are required [27], [28]. The channel coding, RC code and

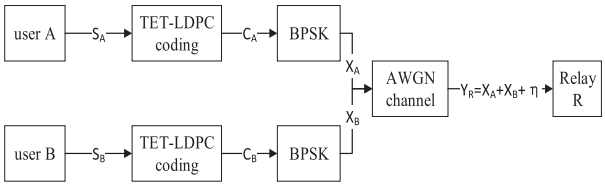

FIGURE 1. System model of JTNC.

PNC code can ensure the communication reliability and boost the throughput of wireless communication systems. However, the research on them is independent of each other still now. Thus, this paper jointly utilizes RC-aided channel coding and PNC techniques for wireless communications. This paper proposes a puncturing scheme named choice of locations and symbols (CLS) for JTNC codes in TWRS. The main contributions of this paper are as follows.

1) First, we propose a JTNC scheme exploiting the performance and implementation advantages of TET-LDPC codes. The corresponding extended LLR decoding algorithm is also investigated to reduce the decoding complexity of JTNC.
2) Second, we develop a CLS puncturing scheme to achieve RC-JTNC for improving transmission efficiency. The simulation results show that the resulting CLS-aided RC-JTNC achieves remarkable performance gains over the existing puncturing algorithms over a wide rate ranges especially at the high coding rate.

The remainder of this paper is organized as follows. Section II presents the system model of JTNC. Section III puts forth the puncturing scheme of JTNC. Section IV shows simulation results of RC-JTNC. Section V concludes this paper.

II. RELATED BACKGROUND

A. SYSTEM MODEL OF JTNC

In this section, we consider TWRS with two users A and B and one relay R. Two users A and B transmit their messages to the relay R simultaneously. With the help of the relay R, users A and B exchange their messages with each other by doing simply XOR operation. Fig. 1 illustrates a system model of JTNC. In this paper, we use a boldface letter to denote a vector and the corresponding italic letter to denote a symbol within the vector. For example, $\mathbf{x}_A$ is a vector, and x_A is a symbol within the vector.

Let $\mathbf{S}_t$, $t \in \{A, B\}$, be a length-K vector over $\{0, 1\}^K$ representing user t's source message. Then, $\mathbf{S}_A$ and $\mathbf{S}_B$ are encoded by the same linear channel code to generate length-N codeword vectors $\mathbf{C}_A$ and $\mathbf{C}_B$ over $\{0, 1\}^N$, respectively. Assume that both users A and B adopt BPSK modulation. Thus, users A and B create two signal vectors $\mathbf{X}_A$ and $\mathbf{X}_B$ for transmission by mapping $\mathbf{C}_A$ and $\mathbf{C}_B$ over $\{-1, +1\}^N$, respectively. Assuming equal powers and frame synchronization between two users, the received signal at the relay is given by

$$\mathbf{Y}_R = \mathbf{X}_A + \mathbf{X}_B + \eta, \tag{1}$$

where η denotes a vector containing i.i.d. white Gaussian noise samples with zero mean and variance of σ^2.

TABLE 1. PNC mapping rules.

C_A	C_B	$C_{A\oplus B}$	C_{A+B}	X_A	X_B	Y_R
0	0	0	0	1	1	2+ η
0	1	1	1	1	-1	η
1	0	1	1	-1	1	η
1	1	0	2	1	-1	-2+η

Table 1 lists PNC mapping rules between user symbols and received symbols. Let $\mathbf{C}_{A\oplus B} = \mathbf{C}_A \oplus \mathbf{C}_B$ denote the XOR output vector of two codewords $\mathbf{C}_A$ and $\mathbf{C}_B$. We can see that $\mathbf{C}_{A\oplus B}$ is also a valid codeword since users A and B employ the same channel coding. Furthermore, denote $\mathbf{C}_{A+B} = \mathbf{C}_A + \mathbf{C}_B$ as the arithmetic sum of $\mathbf{C}_A$ and $\mathbf{C}_B$.

From Table 1, we can see that if $C_{A\oplus B} = 0$, $C_{A+B} = 0$ or 2 and $Y_R = 2 + \eta$ or $-2 + \eta$. If $C_{A\oplus B} = 1$, $C_{A+B} = 1$ and $Y_R = \eta$. The a-priori probability of $C_{A\oplus B} = 0$, 1 and 2, i.e., the a-priori probability of the corresponding received signal $Y_R = 2 + \eta$, η and $-2 + \eta$, are 1/4, 1/2 and 1/4, respectively.

B. TET-LDPC CODES

An LDPC code is a linear block code described by a very sparse parity check matrix H. In LDPC codes, all edges are statistical equivalence in the tanner graph and all nodes are described by their degrees, i.e., the number of edges they are connected to. From a edge perspective [29], LDPC codes are specified by two polynomials $\lambda(z) = \sum_i \lambda_i z^{i-1}$ and $\rho(z) = \sum_i \rho_i z^{i-1}$, where z represents variables, λ_i means the fraction of edges connected to variable nodes (VNs) of degree i and ρ_i means the fraction of edges connected to check nodes (CNs) of degree i [30].

MET-LDPC codes which can yield improvements in performance and error floor are first introduced in [17]. Although MET-LDPC codes are generalizations of the concept of LDPC codes, they are different from LDPC codes. First, MET-LDPC codes with multiple equivalence types of edges set the edge degree as a vector which denotes the number of edges connected to the node from each edge equivalence type independently. Second, MET-LDPC codes can also be represented by two polynomials, but unlike LDPC codes, they are done from a node perspective [29]. The polynomial coefficients of MET-LDPC codes represent the fraction of nodes connected to each edge equivalence type. We introduce our definitions as follows.

Assuming that the MET-LDPC code consists of a finite number n_T of edge types. Let a length-n_T vector $\mathbf{d}$ be a multi-edge degree with d_j being the number of the j-th type edge, $j = 1, 2, \ldots, n_T$. Denote $\mathbf{x}$ as a length-n_T vector, representing variables and x_j as variables associated with the j-th type edge, $j = 1, 2, \ldots, n_T$. The coded bits (VNs) of the

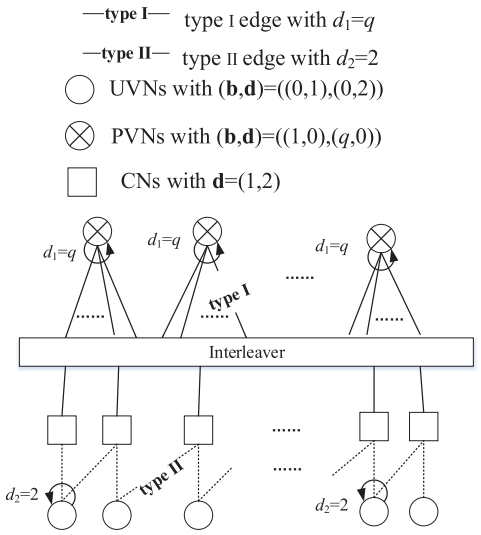

FIGURE 2. Tanner graph representation of TET-LDPC codes.

MET-LDPC code may have different received distributions, i.e., the bits associated to the different edge types may go through different channels. Let n_θ denote the number of different channels. Let $\mathbf{r}$ denote a length-n_θ vector which represents received distributions. In this paper, we focus on two received distributions, r_1 which is used to puncture variables means an erasure channel, and r_2 over which the code bits are transmitted represents the AWGN channel. Let a length-n_θ vector $\mathbf{b}$ be a received degree, which means the received probability associated with the received distribution. Typically, only one symbol in $\mathbf{b}$ is set to 1, and the other symbols are set to 0.

MET-LDPC codes can be described by two polynomials. We denote these polynomials by

$$v(\mathbf{r}, \mathbf{x}) = \sum v_{\mathbf{b},\mathbf{d}} \mathbf{r}^{\mathbf{b}} \mathbf{x}^{\mathbf{d}}, \tag{2}$$

$$\mu(\mathbf{x}) = \sum \mu_{\mathbf{d}} \mathbf{x}^{\mathbf{d}}, \tag{3}$$

where $\mathbf{x}^{\mathbf{d}} = \prod_{i=1}^{n_T} x_i^{d_i}$ and $\mathbf{r}^{\mathbf{b}} = \prod_{j=1}^{n_\theta} r_j^{b_j}$. In the graph, $v_{\mathbf{b},\mathbf{d}}N$ denotes the number of VNs with type $(\mathbf{b}, \mathbf{d})$, $\mu_{\mathbf{d}}N$ denotes the number of CNs with type $\mathbf{d}$, $v(\mathbf{r}, \mathbf{x})$ is associated with VNs and $\mu(\mathbf{x})$ is associated with CNs.

In this paper, a kind of MET-LDPC codes, i.e., TET-LDPC codes are considered. Fig. 2 represents the Tanner graph of TET-LDPC codes, where TET-LDPC codes have two equivalence classes of edges. One is type I with $d_1 = q$, where q means the edge degree of type I, and the other one is type II with $d_2 = 2$. The type I edge and the type II edge are not equivalent class of edges. Two edge classes of TET-LDPC codes divide VNs into two parts, punctured VNs (PVNs) and un-punctured VNs (UVNs). The structure of type I edges connected to PVNs is constructed like regular LDPC codes which can improve decoding threshold. Furthermore, UVNs are connected to type II edges in a accumulate chain, which simplifies encoding and guarantees stability to the structure. Thus, the distribution of PVNs is $(\mathbf{b}, \mathbf{d}) = ((1, 0), (q, 0))$.

TABLE 2. The structure of TET-LDPC codes.

$v_{\mathbf{b},\mathbf{d}}$	**b**	**d**	$\mu_{\mathbf{d}}$	**d**
$1/q$	1 0	q 0	1	1 2
1	0 1	0 2		

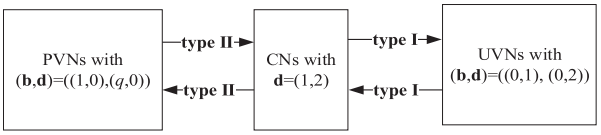

FIGURE 3. The decoding schematic diagram.

In particular, $\mathbf{b} = (1, 0)$ denotes $\mathbf{r}^{\mathbf{b}} = r_1$, which means VNs are transmitted over the erasure channel, i.e., VNs are punctured. The other distribution of UVNs is $(\mathbf{b}, \mathbf{d}) = ((0, 1), (0, 2))$, where $\mathbf{b} = (0, 1)$ denotes $\mathbf{r}^{\mathbf{b}} = r_2$, which means VNs are transmitted over the AWGN channel. The basic degree structure shown in Tab. 2 specifies an instance of TET-LDPC codes. A graph ensemble of TET-LDPC codes can be described by two polynomials as follows.

$$v(\mathbf{r}, \mathbf{x}) = \frac{1}{q} r_1 {x_1}^q + r_2 {x_2}^2, \tag{4}$$

$$\mu(\mathbf{x}) = x_1 {x_2}^2. \tag{5}$$

C. THE LLR DECODING FOR JTNC OVER AWGN CHANNELS

We assume that the same TET-LDPC code is used at two users. Thus, the relay decodes the XOR message with the same Tanner graph as in the users nodes. Due to having two types of VNs, the decoding of TET-LDPC codes is different from the conventional iterative decoding of LDPC codes. Fig. 3 shows the decoding schematic diagram and the LLR messages are iterative updated between the type I edge and the type II edge. Note that that decoding starts with UVNs. From the perspective of edge, we give the decoding steps of TET-LDPC codesas follows.

1) Decoding starts with UVNs.
2) Update the LLR messages passed from UVNs to CNs on type II edges,
3) Update the LLR messages passed from CNs to PVNs on type I edges,
4) Update the LLR messages passed from PVNs to CNs on type I edges,
5) Update the LLR messages passed from CNs to UVNs on type II edges.

Iterative Decoding over $2) - 5)$ steps is stopped if the maximum number of iterations is reached. Next we elaborates the LLR decoding for JTNC.

1) INITIALIZATION

Let $\mathbf{pLch}(n)$ denote the channel LLR message for the n-th VN $\mathbf{C}_{A+B}(n)$, given by

$$\begin{aligned} \mathbf{pLch}(n) &= [pLch_0(n), pLch_2(n)] \\ &= [\log(\frac{p\bar{L}ch_0(n)}{p\bar{L}ch_1(n)}), \log(\frac{p\bar{L}ch_2(n)}{p\bar{L}ch_1(n)})], \end{aligned} \tag{6}$$

where $n = 1, 2, \ldots, N$, and $p\bar{L}ch_i(n)$ denote the probability of $\mathbf{C}_{A+B}(n) = i, i \in \{0, 1, 2\}$. Given the signal $\mathbf{Y}_R(n)$, we consider three cases to compute $p\bar{L}ch_i(n)$ in the followings.

Case 1: $\mathbf{C}_A(n)$ and $\mathbf{C}_B(n)$ are not punctured. $p\bar{L}ch_i(n)$ is computed by

$$\begin{aligned} p\bar{L}ch_0(n) &= \frac{1}{4\sqrt{2\pi}\gamma}\exp(-\frac{(\mathbf{Y}_R(n)-2)^2}{2\sigma^2}),\\ p\bar{L}ch_1(n) &= \frac{1}{2\sqrt{2\pi}\gamma}\exp(-\frac{\mathbf{Y}_R(n)^2}{2\sigma^2}),\\ p\bar{L}ch_2(n) &= \frac{1}{4\sqrt{2\pi}\gamma}\exp(-\frac{(\mathbf{Y}_R(n)+2)^2}{2\sigma^2}), \end{aligned} \tag{7}$$

where γ is a normalization factor to ensure $\sum_{i=0}^{2} p\bar{L}ch_i = 1$.

Case 2: $\mathbf{C}_A(n)$ or $\mathbf{C}_B(n)$ is punctured. Without loss of generality, we assume that $\mathbf{C}_A(n)$ is punctured. Then the received signal $\mathbf{Y}_R(n)$ becomes

$$\mathbf{Y}_R(n) = \mathbf{X}_B(n) + \eta. \tag{8}$$

From Tab. 1, $\mathbf{C}_A(n) = 0$ implies $\mathbf{C}_{A+B}(n) = 0$ or 1 and $\mathbf{X}_A(n) + \mathbf{X}_B(n) = 1 + \mathbf{X}_B(n) = 2$ or 0. If $\mathbf{C}_A(n) = 1$, then $\mathbf{C}_{A+B}(n) = 1$ or 2 and $\mathbf{X}_A(n)+\mathbf{X}_B(n) = 1+\mathbf{X}_B(n) = 0$ or -2. Thus, with the punctured $\mathbf{C}_A(n)$, we have

$$\begin{aligned} p\bar{L}ch_0(n) &= \frac{1}{4\sqrt{2\pi}\gamma}\exp(-\frac{((\mathbf{Y}_R(n)+1)-2)^2}{2\sigma^2})\\ &= \frac{1}{4\sqrt{2\pi}\gamma}\exp(-\frac{(\mathbf{Y}_R(n)-1)^2}{2\sigma^2}),\\ p\bar{L}ch_1(n) &= \frac{1}{4\sqrt{2\pi}\gamma}\exp(-\frac{(\mathbf{Y}_R(n)+1)^2}{2\sigma^2})\\ &\quad+\frac{1}{4\sqrt{2\pi}\gamma}\exp(-\frac{(\mathbf{Y}_R(n)-1)^2}{2\sigma^2}),\\ p\bar{L}ch_2(n) &= \frac{1}{4\sqrt{2\pi}\gamma}\exp(-\frac{((\mathbf{Y}_R(n)-1)+2)^2}{2\sigma^2})\\ &= \frac{1}{4\sqrt{2\pi}\gamma}\exp(-\frac{(\mathbf{Y}_R(n)+1)^2}{2\sigma^2}), \end{aligned} \tag{9}$$

where γ is a normalization factor.

Case 3: Both $\mathbf{C}_A(n)$ and $\mathbf{C}_B(n)$ are punctured. In this case, $p\bar{L}ch_0(n) = \frac{1}{4}, p\bar{L}ch_1(n) = \frac{1}{2}$ and $p\bar{L}ch_2(n) = \frac{1}{4}$. Then the channel LLR message $\mathbf{pLch}(n) = [pLch_0(n), pLch_2(n)] = [\log(0.5), \log(0.5)]$.

Next, we show LLR messages update on different types of edges. To facilitate describing decoding, we define two functions Ω and $\bar{\Omega}$. Assume that two inputs $\mathbf{w} = [w_0, w_2]$ and $\mathbf{g} = [g_0, g_2]$ arrive at a CN. Then the output LLR message from the CN is $\mathbf{f} = [f_0, f_2]$, where

$$\begin{aligned} f_0 &= \Omega(w_0, g_0, w_2, g_2)\\ &= \log(\exp(w_0+g_0)+\exp(w_2+g_2)+0.5)\\ &\quad-\log(\exp(w_0)+\exp(w_2)+\exp(g_0)+\exp(g_2)), \end{aligned} \tag{10}$$

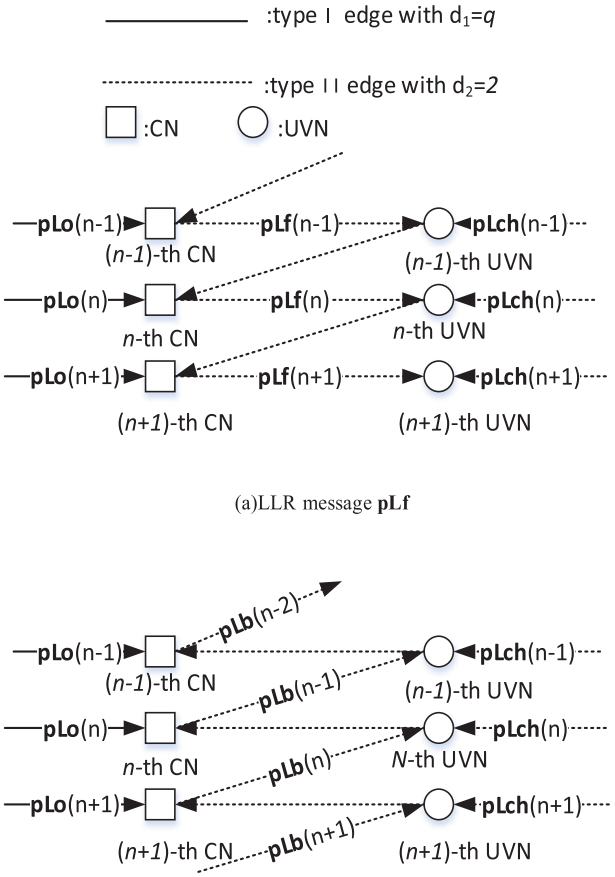

FIGURE 4. LLR messages update on the type II edge. (a)LLR message **pLf**. (b)LLR message **pLb**.

and

$$\begin{aligned} f_2 &= \bar{\Omega}(w_0, g_0, w_2, g_2)\\ &= \log(\exp(w_0+g_2)+\exp(w_2+g_0)+0.5)\\ &\quad-\log(\exp(w_0)+\exp(w_2)+\exp(g_0)+\exp(g_2)). \end{aligned} \tag{11}$$

2) LLR MESSAGES UPDATING ON THE TYPE II EDGE WITH $d_2 = 2$

Fig. 4 shows the factor graph of messages update on the type II edge. We denote $\mathbf{pLf}(n) = [pLf_0(n), pLf_2(n)]$ as the LLR message from the $(n-1)$-th CN to the n-th UVN on the type II edge. Denote $\mathbf{pLo}(n) = [pLo_0(n), pLo_2(n)]$ as the LLR message from the n-th PVN to the n-th CN over the type I edge, $n = 1, 2, \ldots, N$. The $\mathbf{pLf}(n)$ can be computed by

$$\begin{aligned} &pLf_0(n)\\ &= \Omega((pLf_0(n-1)+pLch_0(n-1)+\log(2.0)), pLo_0(n),\\ &\quad(pLf_2(n-1)+pLch_2(n-1)+\log(2.0)), pLo_2(n)), \end{aligned} \tag{12}$$

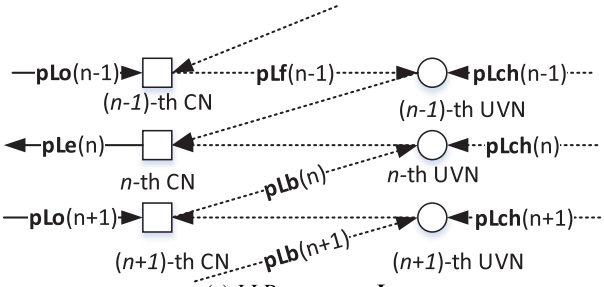

(a) LLR message **pLe**

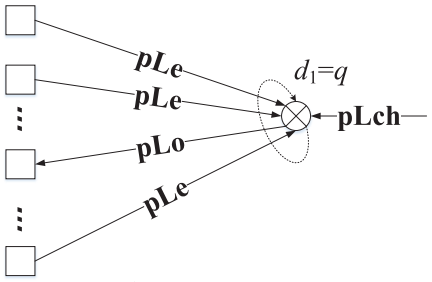

(b) LLR message **pLo**

FIGURE 5. LLR messages updating on the type I edge. (a)LLR message **pLe**. (b)LLR message **pLo**.

and

$$\begin{aligned} &pLf_2(n) \\ &= \bar{\Omega}((pLf_0(n-1)+pLch_0(n-1)+\log(2.0)), pLo_0(n), \\ &\quad (pLf_2(n-1)+pLch_2(n-1)+\log(2.0)), pLo_2(n)). \end{aligned} \tag{13}$$

Moreover, $\mathbf{pLb}(n) = [pLb_0(n), pLb_2(n)]$ denotes the LLR message from the n-th CN to the n-th UVN over the type II edge, given by

$$\begin{aligned} &pLb_0(n) \\ &= \Omega((pLb_0(n+1)+pLch_0(n+1)+\log(2.0)), pLo_0(n+1), \\ &\quad (pLb_2(n+1)+pLch_2(n+1)+\log(2.0)), pLo_2(n+1)), \end{aligned} \tag{14}$$

and

$$\begin{aligned} &pLb_2(n) \\ &= \bar{\Omega}((pLb_0(n+1)+pLch_0(n+1)+\log(2.0)), pLo_0(n+1), \\ &\quad (pLb_2(n+1)+pLch_2(n+1)+\log(2.0)), pLo_2(n+1)). \end{aligned} \tag{15}$$

3) LLR MESSAGES UPDATE OVER THE TYPE I EDGE WITH $d_1 = q$

Fig. 5 shows the factor graph of LLR messages update over the type I edge.

Let $\mathbf{pLe}(n) = [pLe_0(n), pLe_2(n)]$ denote the LLR message out of CNs over the type I edge. Then, $\mathbf{pLe}(n)$ can be calculated by

$$\begin{aligned} pLe_0(n) = \Omega&((pLf_0(n-1)+pLch_0(n-1)+\log(2.0)), \\ &\times(pLb_0(n)+pLch_0(n)+\log(2.0)), \\ &\times(pLf_2(n-1)+pLch_2(n-1)+\log(2.0)), \\ &\times(pLb_2(n)+pLch_2(n)+\log(2.0))), \end{aligned} \tag{16}$$

and

$$\begin{aligned} pLe_2(n) = \bar{\Omega}&((pLf_0(n-1)+pLch_0(n-1)+\log(2.0)), \\ &\times(pLb_0(n)+pLch_0(n)+\log(2.0)), \\ &\times(pLf_2(n-1)+pLch_2(n-1)+\log(2.0)), \\ &\times(pLb_2(n)+pLch_2(n)+\log(2.0))). \end{aligned} \tag{17}$$

Because the VN is punctured in Fig. 5(b), the channel LLR message is $\mathbf{pLch} = [pLch0, pLch2] = [\log(0.5), \log(0.5)]$. Then $\mathbf{pLo}(n)$ is calculated by

$$\begin{aligned} &pLo_0(n) \\ &= (q-1)\times\log(2.0) + \sum_{\substack{j=1 \\ j\neq(n \bmod q)}}^{q} pLe_0(\lceil\frac{n}{q}\rceil\times q+j)+\log(0.5), \end{aligned} \tag{18}$$

$$\begin{aligned} &pLo_2(n) \\ &= (q-1)\times\log(2.0) + \sum_{\substack{j=1 \\ j\neq(n \bmod q)}}^{q} pLe_2(\lceil\frac{n}{q}\rceil\times q+j)+\log(0.5), \end{aligned} \tag{19}$$

where $\lceil\rceil$ denotes integer ceil.

4) JTNC MAPPING

For VN, we define the *a-prosteriori* LLR vector $\mathbf{p}(m) = [p_0(m), p_2(m)]$, which is evaluated by all LLR messages from CNs and the channel LLR message as

$$p_0(m) = \log(0.5)+q\times\log(2.0)+\sum_{j=1}^{q} pLe_0((m-1)\times q+j), \tag{20}$$

and

$$p_2(m) = \log(0.5)+q\times\log(2.0)+\sum_{j=1}^{q} pLe_2((m-1)\times q+j), \tag{21}$$

where $m = 1, 2, \ldots, K$, Furthermore, the JTNC mapping based on LLR messages is given by:

$$\hat{\mathbf{S}}_{A\oplus B}(m) = \begin{cases} 0, & \text{if } \max(p_0(m), p_2(m)) \leq 0, \\ 1, & \text{otherwise.} \end{cases} \tag{22}$$

Fig. 6 plots the BER of the JTNC decoder with different block lengths at coding rates of 0.5 and 0.2, respectively. As expected, the JTNC scheme with longer block length or lower rate performs better than those with shorten length or higher rate.

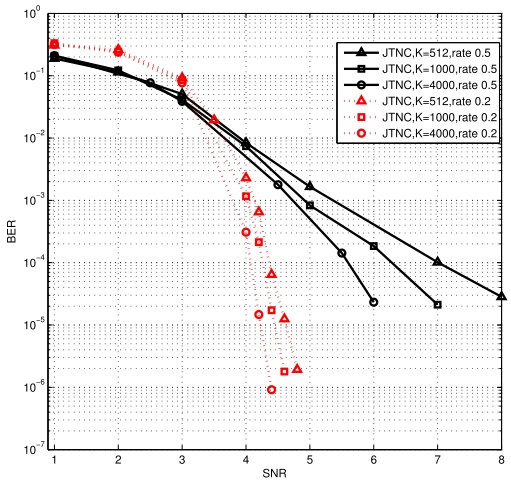

FIGURE 6. The BER performance of JTNC with rates of 0.2 and 0.5.

III. THE PUNCTURING SCHEME FOR JTNC

The puncturing scheme is an effective way to realized RC codes which can be encoded and decoded from a single mother code. This section constructs the puncturing scheme for JTNC, which mainly consists of two steps:

1) Select a puncturing location in TWRS;
2) Select punctured symbols of JTNC in the location chosen in step 1).

The resulting puncturing scheme named choice of locations and symbols (CLS) is described as follows.

A. THE CHOICE OF PUNCTURING LOCATIONS IN TWRS

Denote R_m as the mother code rate and R_g as the target rate of JTNC. Let N_{pum} be the number of punctured VNs, computed by

$$\begin{aligned} N_{pum} &= N \times (1 - \frac{R_m}{R_g}) \\ &= K \times (\frac{1}{R_m} - \frac{1}{R_g}). \end{aligned} \tag{23}$$

As a two stages transmission, TWRS have two users A and B, and one relay R. Therefore, we consider three different puncture locations, at user A or user B (AOB), at user A and user B (AAB), and at the relay R (RP). It needs to compare three location puncture schemes in TWRS. Three schemes are summarized as follows.

1) AOB SCHEME

Fig. 7 shows that we deliberately puncture $2N_{pum}$ UVNs at user A or user B to achieve RC-JTNC. Let $\bar{\mathbf{C}}_t$ denote a punctured codeword from $\mathbf{C}_t$, $t \in \{A, B\}$.

Denote N_{C_t} as the number of PVNs in $\mathbf{C}_t$, $t \in \{A, B\}$. In AOB scheme, there are two cases, one is $N_{C_A} = 2N_{pum}, N_{C_B} = 0$, the other one is $N_{C_A} = 0, N_{C_B} = 2N_{pum}$.

TABLE 3. Several different code rate transmission schemes.

R_g	user A		user B	
	R_A	N_{C_A}	R_B	N_{C_B}
0.4	$\frac{8}{17}$	448	$\frac{8}{23}$	64
	$\frac{8}{18}$	384	$\frac{8}{22}$	128
	$\frac{8}{19}$	320	$\frac{8}{21}$	192
	$\frac{8}{20}$	256	$\frac{8}{20}$	256

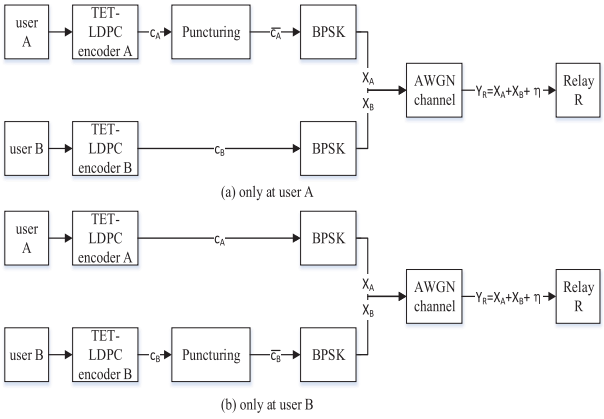

FIGURE 7. AOB scheme.

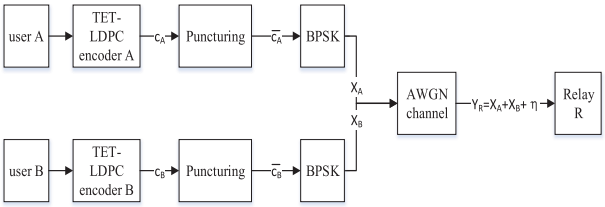

FIGURE 8. AAB scheme.

2) AAB SCHEME

In this case, we puncture the total $2N_{pum}$ UVNs at user A and user B, as shown in Fig. 8. It has to satisfy

$$N_{C_A} + N_{C_B} = 2N_{pum}. \tag{24}$$

Moreover, we consider that punctured nodes of user A and user B are different to achieve different code rates for transmission. Given $R_m = 0.3$ and $K = 512$. Let R_t denote the target code rate of user t. Tab. 3 shows four transmission schemes with different R_t.

Fig. 9 shows the BER performance of four schemes over AWGN channels. We can see that AAB has the best performance when $N_{C_A} = N_{C_B}$, i.e., $R_A = R_B$. Note that the other schemes can be applied when channel conditions of user A and user B are different.

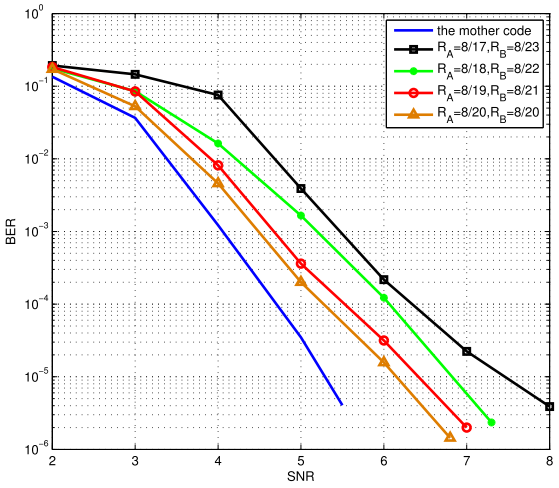

FIGURE 9. BERs of RC-JTNC designed by AAB scheme at difference code rates, $K = 512$.

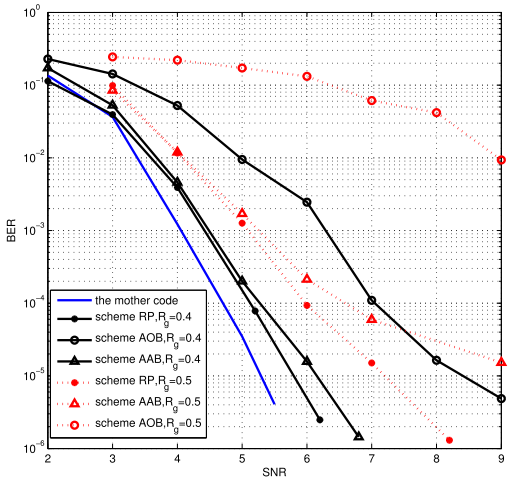

FIGURE 11. BERs of RC-JTNC achieved by three puncturing schemes, $K = 512$.

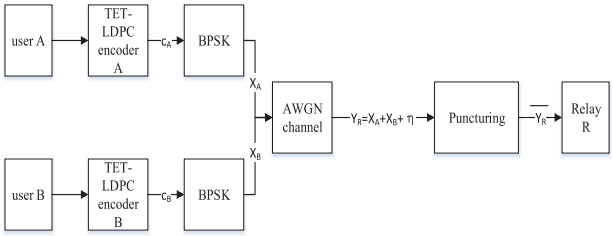

FIGURE 10. RP scheme.

3) RP SCHEME

Fig. 10 shows that we puncture N_{pum} UVNs from $\mathbf{Y}_R$ at the relay R. In this case, $N_{C_A} = 0$ and $N_{C_B} = 0$, but the puncturing symbol at the relay $N_{Y_R} = N_{pum}$.

Fig. 11 compares the BER performance of AAB, AOB, and RP schemes in JTNC with $R_m = 0.3$ and $K = 512$. Random puncturing algorithm is applies for three schemes. The simulation results shows that RP performs better than AAB, and AOB performs the worst among three schemes. At the BER of 10^{-6}, RP-based RC-JTNC has a gain of 0.5 dB performance over AAB at rate of 0.4. In particular, this gain is increased to more than 2 dB at rate of 0.5. The RP also provides a gain of 3 dB over AOB at rate 0.4 and the gain is larger at rate of 0.5. Thus, we next consider the RP scheme to achieve RC-JTNC.

B. THE CHOICE OF PUNCTURED SYMBOLS IN JTNC

TET-LDPC codes are constructed from the node perspective. Thus, the puncture algorithm for JTNC needed to be carefully designed from the node perspective rather than the edge perspective in conventional channel codes.

In TET-LDPC codes, PVNs connected to type I edges are transmitted over an erasure channel. Thus, if we want to puncture VNs, we can puncture the remaining UVNs connected to type II edges. We introduce the following notations.

Let M_α, $\alpha \in \{0, 1, 2, 3, 4\}$ denote four VNs and T_β, $\beta \in \{1, 2\}$ denote two CNs. M_0, M_2 and M_4 are connected to type II edges and the degree distribution is $(\mathbf{b}, \mathbf{d}) = ((0, 1), (0, 2))$. M_1 and M_3 with degree distribution $(\mathbf{b}, \mathbf{d}) = ((1, 0), (q, 0))$ are connected to type I edges. Fig. 12 shows that M_0 is connected to T_1 and T_2 by type II edges. M_1 and T_1, M_3 and T_2 are connected by type I edges, respectively. M_2 and T_1, M_4 and T_2 are connected by type II edges, respectively.

Let $\mathbf{L}^{\beta\alpha} = [L_0^{\beta\alpha}, L_2^{\beta\alpha}]$ denote the LLR message from the β-th CN to the α-th VN. Let $\hat{\mathbf{L}}^{\alpha\beta} = [\hat{L}_0^{\alpha\beta}, \hat{L}_2^{\alpha\beta}]$ denote the LLR message from the α-th VN to the β-th CN.

The LLR message passed from T_1 to M_0 can be calculated by

$$\mathbf{L}^{10} = [L_0^{10}, L_2^{10}] \tag{25}$$

where

$$L_0^{10} = \Omega(\hat{L}_0^{11}, \hat{L}_0^{21}, \hat{L}_2^{11}, \hat{L}_2^{21}), \tag{26}$$

and

$$L_2^{10} = \bar{\Omega}(\hat{L}_0^{11}, \hat{L}_0^{21}, \hat{L}_2^{11}, \hat{L}_2^{21}). \tag{27}$$

In Fig. 12, M_1 is punctured before transmission, and we have $\bar{\mathbf{L}}^{11} = [\hat{L}_0^{11}, \hat{L}_2^{11}] = [\log(0.5), \log(0.5)]$. There are two cases to compute LLR messages with PVNs.

Case 1: As shown in Fig. 13, M_2 is also punctured. In this case, we have $\hat{\mathbf{L}}^{21} = \hat{\mathbf{L}}^{11} = [\log(0.5), \log(0.5)]$ at the first iteration, and L_0^{10} and L_2^{10} are given by

$$L_0^{10} = L_2^{10} = \log(0.5). \tag{28}$$

Thus, the LLR message passed from T_1 to M_0 is not reliable. Since the edge degree of M_0 is 2 and M_4 is un-punctured, M_0 can obtain message from M_4. In other words, L_0^{20} and L_2^{20} are not equal to $\log(0.5)$, providing useful messages for M_0. Fig. 13 also shows that M_3 is punctured before transmission. Thus we have $\bar{\mathbf{L}}^{32} = [\hat{L}_0^{32}, \hat{L}_2^{32}] = [\log(0.5), \log(0.5)]$, and

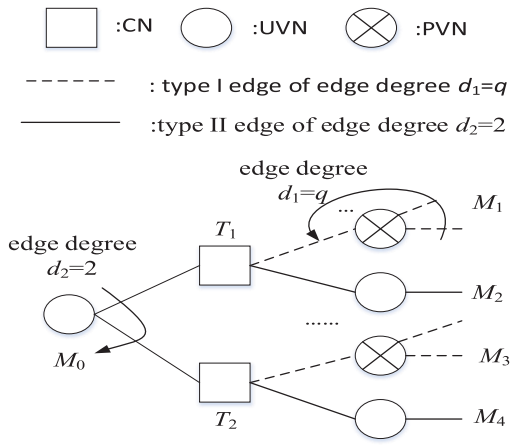

FIGURE 12. The structure of VNs connected the type II edge.

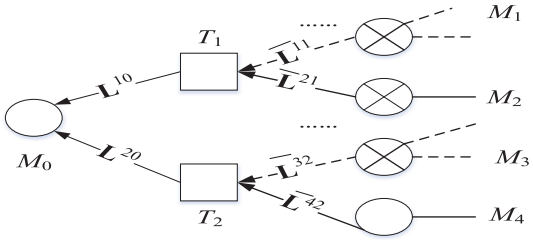

FIGURE 13. LLR message update with punctured M_2.

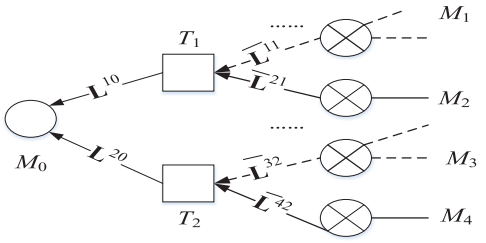

FIGURE 14. LLR messages update with punctured M_2 and M_4.

L_0^{20} and L_2^{20} can be computed by

$$L_0^{20} = \Omega(\hat{L}_0^{32}, \hat{L}_0^{42}, \hat{L}_2^{32}, \hat{L}_2^{42}) \neq \log(0.5), \tag{29}$$

and

$$L_2^{20} = \bar{\Omega}(\hat{L}_0^{32}, \hat{L}_0^{42}, \hat{L}_2^{32}, \hat{L}_2^{42}) \neq \log(0.5). \tag{30}$$

The PVNs M_1, M_2 and M_3, can be recovered by the LLR message from the VN M_4.

Case 2: As shown in Fig. 14, both M_2 and M_4 are punctured. Then we have $\hat{\mathbf{L}}^{42} = [\hat{L}_0^{42}, \hat{L}_2^{42}] = [\log(0.5), \log(0.5)]$. Thus, L_0^{20} and L_2^{20} can be computed by

$$L_0^{20} = \Omega(\hat{L}_0^{32}, \hat{L}_0^{42}, \hat{L}_2^{32}, \hat{L}_2^{42}) = \log(0.5), \tag{31}$$

and

$$L_2^{20} = \bar{\Omega}(\hat{L}_0^{32}, \hat{L}_0^{42}, \hat{L}_2^{32}, \hat{L}_2^{42}) = \log(0.5). \tag{32}$$

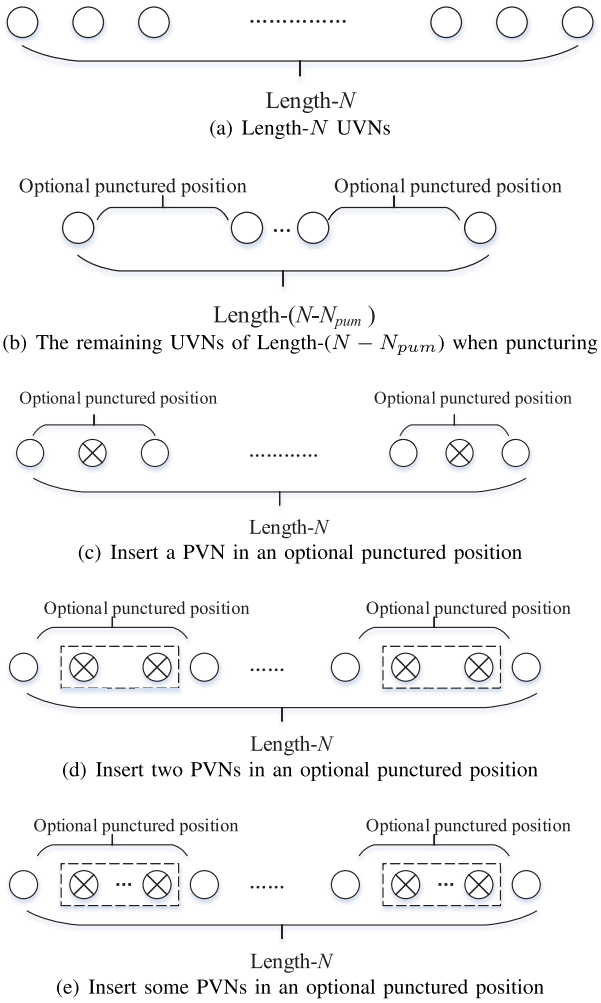

FIGURE 15. The patterns of puncturing in RC-JTNC. (a) Length-N UVNs. (b) The remaining UVNs of Length-(N - N_{pum}) when puncturing.

Then, we have

$$\mathbf{L}^{20} = \mathbf{L}^{10} = [\log(0.5), \log(0.5)]. \tag{33}$$

The message of the VN M_0 is only the sum of channel messages of two PVNs. The PVNs M_1, M_2, M_3 and $M4$ cannot be recovered without receiving other messages, i.e.,

$$L_0^{11} = L_0^{12} = L_0^{23} = L_0^{24} = L_2^{11} = L_2^{12} = L_2^{23} = L_2^{24} = \log(0.5). \tag{34}$$

Moreover, as iterative decoding proceeds, the unreliable message passed in the decoder has a great impact on decoding. To recover M_0, we should ensure that at least one of four VNs connected to M_0 by CNs is not punctured. In other words, a PVN can be recovered when at least one of four VNs connected to it by CNs is not punctured.

Since that we have two types of VNs in the JTNC, i.e, PVNs and UVNs, we can puncture UVNs to achieve RC-JTNC. Fig. 15. shows patterns of puncture which can be successful recovered in the decoding. Fig. 15(a) shows

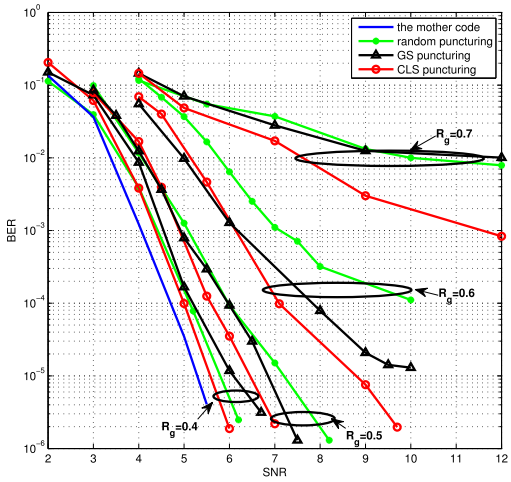

FIGURE 16. BER performance of RC-JTNCs with random puncturing, GS puncturing and CLS puncturing schemes, respectively.

length-N UVNs that can be punctured. Fig. 15(b) shows the remaining UVNs of Length-$(N - N_{pum})$ after puncturing. Denote the position between two UVNs as an optional punctured position. Some optional punctured positions may be selected to insert PVNs. Fig. 15(c) and Fig. 15(d) show that we simply insert one and two PVNs at the selected optional punctured positions, respectively. In both cases, at least one UVN can be guaranteed to be connected to one VN. However, as the number of inserted PVNs increases, it is not guaranteed that at least one UVN is connected to one VN, as shown in Fig. 15(e).

C. THE PROPOSED PUNCTURING ALGORITHM FOR JTNC

We summarize the proposed puncturing algorithm CLS for JTNC as follows.

1) Choice of the puncturing locations:
In TWRS, we select the RP scheme as the puncturing location scheme to achieve RC-JTNC.
2) Initialization:
We compute N_{pum} from (23). The patterns of puncturing are shown in the Fig. 15. There are at most two PVNs inserted in the optional punctured position. The number of optional punctured positions N_L is calculated by

$$N_L = K \times (\frac{1}{R_g}) - 1. \tag{35}$$

3) Puncturing:
   a) If $N_{pum} \leq N_L$, go on to b); if $N_{pum} > N_L$, go to c).
   b) Randomly select N_{pum} non-repeating positions from N_L optional punctured positions. Insert a PVN in each of these selected positions.
   Go to 4).
   c) Count the max number of PVNs I_{max} in the optional punctured position by (36). Count the max number of positions P_{max} selected from optional punctured positions by (37).

$$I_{max} = \lceil \frac{N_{pum}}{N_L} \rceil, \tag{36}$$

$$P_{max} = \lceil \frac{N_{pum}}{I_{max}} \rceil. \tag{37}$$

Randomly select P_{max} non-repeating positions from N_L optional punctured positions. Insert I_{max} PVNs at the first $(P_{max} - 1)$ positions and P_{num} PVNs at the last position, where P_{num} is calculated by

$$P_{num} = N_{pum} - I_{max} \times (P_{max} - 1). \tag{38}$$

Go to 4).
4) The end of CLS for JTNC.

Note that at the beginning of the CLS algorithm, we insert PVNs at the optional punctured positions and the number of PVNs should be as small as possible. Thus, we can realize RC codes with continuous rates by puncturing VNs one by one in the proposed CLS. We pick a single RC-JTNC which has an excellent performance across a range of rates.

IV. SIMULATION RESULTS

This section illustrates the performance of the proposed RC-JTNC. For comparison, we also plot the performance of the RC codes achieved by random puncturing [31] and the GS puncturing algorithm [24], [26]. Fig. 16 shows the resulting BER performance.

The simulated block length are 1280, 1024, 853, 731, 640 and 569 with $R_g = 0.4, 0.5, 0.6, 0.7, 0.8$ and 0.9, respectively. From Fig. 16, we can see that with few PVNs, i.e., $R_g = 0.4$, the three schemes perform almost the same at low SNR regime, while CLS achieves a gain of 0.2 dB and 0.8 dB over random puncturing algorithm and GS algorithm, respectively, at high SNR regime, i.e, at the BER of 10^{-6}.

As the rate increases, the proposed RC-JTNC starts to show larger gains over the two other schemes. We can observe that CLS has a gain of 0.3 dB over GS algorithm, and this gain increases to 1 dB over random puncturing algorithm at $R_g = 0.5$. The gains of CLS over random puncturing and GS schemes are 1 dB and 3 dB respectively at $R_g = 0.6$. The gain can be up to 4 dB over both schemes at $R_g = 0.7$.

We can also see that the CLS exhibits a high error-floor at $R_g = 0.7$ when SNR is greater than 7 dB. This is because that too many VNs are punctured in this case. The ratio of PVNs to UVNs (PTU) is $\frac{805}{731} = 1.1 > 1$. In this case, we cannot guarantee all PVNs to be recovered, which leads to a degraded performance for RC-JTNC at the high rate.

V. CONCLUSION

In this paper, we first proposes a TET-LDPC coded JTNC scheme with the aid of PNC technique. Second, we propose a CLS puncturing algorithm to achieve RC-JTNC which considers the choices of puncturing locations and the puncturing symbols of JTNC. Simulation results demonstrate that the proposed RC-JTNC with CLS can provide a family of good RC codes at rates from 0.3 to 0.7, and show considerable

performance gains over the existing puncturing algorithms, especially at the high coding rate.

REFERENCES

[1] R. Ahlswede, N. Cai, S.-Y. R. Li, and R. W. Yeung, "Network information flow," *IEEE Trans. Inf. Theory*, vol. 46, no. 4, pp. 1204–1216, Jul. 2000.

[2] S. Zhang, S. C. Liew, and P. P. Lam, "Hot topic: Physical-layer network coding," in *Proc. MobiCom*, Los Angeles, CA, USA, Jun. 2006, pp. 358–365.

[3] P. Chen, S. C. Liew, and L. Shi, "Bandwidth-efficient coded modulation schemes for physical-layer network coding with high-order modulations," *IEEE Trans. Commun.*, vol. 65, no. 1, pp. 147–160, Jan. 2017.

[4] L. Shi, T. Yang, K. Cai, P. Chen, and T. Guo, "On MIMO linear physical-layer network coding: Full-rate full-diversity design and optimization," *IEEE Trans. Wireless Commun.*, vol. 17, no. 5, pp. 3498–3511, Mar. 2018.

[5] L. Shi and S. C. Liew, "Complex linear physical-layer network coding," *IEEE Trans. Inf. Theory*, vol. 63, no. 8, pp. 4949–4981, Aug. 2017.

[6] L. Shi, S. C. Liew, and L. Lu, "On the subtleties of q-PAM linear physical-layer network coding," *IEEE Trans. Inf. Theory*, vol. 62, no. 5, pp. 2520–2544, Mar. 2016.

[7] L. Lu, T. Wang, S. C. Liew, and S. Zhang, "Implementation of physical-layer network coding," in *Proc. IEEE ICC*, Jun. 2012, pp. 4734–4740.

[8] L. Lu and S. C. Liew, "Asynchronous physical-layer network coding," *IEEE Trans. Wireless Commun.*, vol. 11, no. 2, pp. 819–831, Feb. 2012.

[9] S. Zhang and S.-C. Liew, "Channel coding and decoding in a relay system operated with physical-layer network coding," *IEEE J. Sel. Areas Commun.*, vol. 27, no. 5, pp. 788–796, Jun. 2009.

[10] P. Chen and L. Wang, "A serial joint channel and physical layer network decoding in two-way relay networks," *IEEE Commun. Lett.*, vol. 16, no. 6, pp. 769–772, Jun. 2012.

[11] T. Ferrett and M. C. Valenti, "Noncoherent LDPC-coded physical-layer network coding using multitone FSK," *IEEE Trans. Commun.*, vol. 66, no. 6, pp. 2384–2395, Jun. 2018.

[12] B. Nazer and M. Gastpar, "Reliable physical layer network coding," *Proc. IEEE*, vol. 99, no. 3, pp. 438–460, Mar. 2011.

[13] D. Wubben and Y. Lang, "Generalized sum-product algorithm for joint channel decoding and physical-layer network coding in two-way relay systems," in *Proc. GLOBECOM*, Miami, FL, USA, Dec. 2010, pp. 1–5.

[14] P. Chen, L. Shi, S. C. Liew, Y. Fang, and K. Cai, "Channel decoding for nonbinary physical-layer network coding in two-way relay systems," *IEEE Trans. Veh. Technol.*, vol. 68, no. 1, pp. 628–640, Jan. 2019.

[15] P. Chen, Y. Fang, L. Wang, and F. C. M. Lau, "Decoding generalized joint channel coding and physical network coding in the LLR domain," *IEEE Signal Process. Lett.*, vol. 20, no. 2, pp. 121–124, Feb. 2013.

[16] T. Richardson and R. Urbanke, *Modern Coding Theory*. Cambridge, U.K.: Cambridge Univ. Press, 2008.

[17] T. J. Richardson and R. L. Urbanke. *Multi-Edge Type LDPC Codes*. Accessed: Jan. 2002. [Online]. Available: https://www.researchgate.net/publication/37439748_Multi-edge_type_LDPC_codes

[18] J. Ha, J. Kim, D. Klinc, and S. W. McLaughlin, "Rate-compatible punctured low-density parity-check codes with short block lengths," *IEEE Trans. Inf. Theory*, vol. 52, no. 2, pp. 728–738, Feb. 2006.

[19] R. Garzón-Bohórquez, C. A. Nour, and C. Douillard, "Protograph-based interleavers for punctured turbo codes," *IEEE Trans. Commun.*, vol. 66, no. 5, pp. 1833–1844, May 2018.

[20] J. B. Cain, G. C. Clark, and J. M. Geist, "Punctured convolutional codes of rate *(n-1)/n* and simplified maximum likelihood decoding," *IEEE Trans. Inf. Theory*, vol. IT-25, no. 1, pp. 97–100, Jan. 1979.

[21] J. Hagenauer, "Rate-compatible punctured convolutional codes (RCPC codes) and their applications," *IEEE Trans. Commun.*, vol. COMM-36, no. 4, pp. 389–400, Apr. 1988.

[22] G. Yue, X. Wang, and M. Madihian, "Design of rate-compatible irregular repeat accumulate codes," *IEEE Trans. Commun.*, vol. 55, no. 6, pp. 1153–1163, Jun. 2007.

[23] Y. Fang, Y. L. Guan, G. Bi, L. Wang, and F. C. M. Lau, "Rate-compatible root-protograph LDPC codes for quasi-static fading relay channels," *IEEE Trans. Veh. Technol.*, vol. 65, no. 4, pp. 2741–2747, Apr. 2016.

[24] Y. Fang, G. Bi, Y. L. Guan, and F. C. M. Lau, "A survey on protograph LDPC codes and their applications," *IEEE Commun. Surveys Tuts.*, vol. 17, no. 4, pp. 1989–2016, 4th Quart., 2015.

[25] Y. Zhang, K. Peng, Z. Chen, and J. Song, "Progressive matrix growth algorithm for constructing rate-compatible length-scalable raptor-like quasi-cyclic LDPC codes," *IEEE Trans. Broadcast.*, vol. 64, no. 4, pp. 816–829, Dec. 2018.

[26] Y. You, M. Xiao, and L. Wang, "The rate-compatible multi-edge type LDPC codes with short block length," in *Proc. Int. Conf. WICOM*, Beijing, China, Sep. 2009, pp. 1–4.

[27] G. Cai, Y. Fang, G. Han, J. Xu, and G. Chen, "Design and analysis of relay-selection strategies for two-way relay network-coded DCSK systems," *IEEE Trans. Veh. Technol.*, vol. 67, no. 2, pp. 1258–1271, Feb. 2018.

[28] G. Cai, Y. Fang, G. Han, L. Wang, and G. Chen, "New hierarchical M-ary DCSK communication system: Design and analysis," *IEEE Access*, vol. 5, pp. 17414–17424, 2017.

[29] A. Balatsoukas-Stimming, "Design of LDPC codes for the unequal power two-user Gaussian multiple access channel," Ph.D. dissertation, Dept. Elect. Comput. Eng., Tech. Univ. Crete, Chania, Greece, Jun. 2012.

[30] R. G. Gallager, "Low-density parity-check codes," *IRE Trans. Inf. Theory*, vol. 8, no. 1, pp. 21–28, Jan. 1962.

[31] D. G. M. Mitchell, M. Lentmaier, A. E. Pusane, and D. J. Costello, "Randomly punctured LDPC codes," *IEEE J. Sel. Areas Commun.*, vol. 34, no. 2, pp. 408–421, Feb. 2016.

YING YOU received the M.S. degrees in communication and information systems from Xiamen University, China, in 2010. She is currently a Lecturer with the Fuqing Branch of Fujian Normal University, China. She is also a Visiting Scholar with Fuzhou University, China. Her primary research interests include channel coding, physical layer network coding, and network coding.

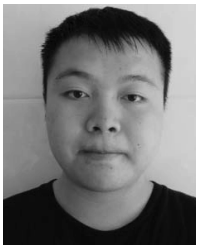

ZHAOPENG XIE received the B.E. degree in electronic engineering from Hubei University, China, in 2009. He is currently pursuing the master's degree in electrical engineering with Fuzhou University, China.

PINGPING CHEN (M'15) received the Ph.D. degree in electronic engineering from Xiamen University, China, in 2013. In 2012, he was a Research Assistant in electronic and information engineering with The Hong Kong Polytechnic University, Hong Kong. From 2013 to 2015, he was a Postdoctoral Fellow with the Institute of Network Coding, The Chinese University of Hong Kong, Hong Kong. He is currently a Professor with Fuzhou University, China. His primary research interests include channel coding, joint source and channel coding, network coding, and UWB communications.

ZHIJIAN LIN received the B.S. and M.S. degrees in communication engineering from Xiamen University, Xiamen, China, in 2004 and 2011, respectively, where he is currently pursuing the Ph.D. degree. His current research interests are mainly in wireless communications and networking. He currently works on device-to-device communications and full-duplex by utilizing the tools of stochastic geometry.